Ocean water vapor and cloud liquid water trends from 1992 to 2005 TOPEX Microwave Radiometer data

S. Keihm,[1] S. Brown,[1] J. Teixeira,[1] S. Desai,[1] W. Lu,[1] E. Fetzer,[1] C. Ruf,[2] X. Huang,[2] and Y. Yung[3]

Received 30 March 2009; revised 18 May 2009; accepted 5 June 2009; published 16 September 2009.

[1] The continuous 1992–2005 data set of the TOPEX Microwave Radiometer (TMR) has been reprocessed to provide global, zonal, and regional scale histories of overocean integrated water vapor (IWV) and cloud liquid water (CLW). Results indicate well-defined trends in IWV on global and hemisphere scales, with values of 1.8 ± 0.4%/decade (60°S–60°N), 2.4 ± 0.4%/decade (0–60°N), and 1.0 ± 0.5%/decade (0–60°S). The uncertainties represent 1 standard deviation of the regressed slope parameter adjusted for lag 1 autocorrelation. These results are comparable to earlier results based on analyses of the multiinstrument SSM/I ocean measurements beginning in 1988. For the 1992–2005 interval, comparisons between SSM/I- and TMR-derived IWV trends show remarkable agreement, with global trends differing by less than 0.3%/decade, comparable to the statistical uncertainty level and about one-sixth of the global TMR-derived trend. Latitudinal and regional analyses of IWV trends show large variability about the global mean, with synoptic scale variations of IWV trends ranging from ∼−8 to +8%/decade. Averaged over 5° latitude bands the IWV trends reveal a near zero minimum in the Southern Tropical Pacific and maximum values of ∼4%/decade over the 30–40N latitude band. Comparisons with band latitude averaged SST data over the same 1992–2005 interval roughly match a delta_IWV/delta_SST trend scaling of ∼11%/K, consistent with previously observed tropical and midlatitude seasonal variability. TMR-derived CLW trends are fractionally comparable to the IWV trends. The CLW values are 1.5 ± 0.6%/decade (60°S–60°N), 2.0 ± 0.8%/decade (0–60°N), and 1.1 ± 0.8%/decade (0–60°S). When scaled to global mean CLW derived from SSM/I and compared seasonally, the TMR CLW variations exhibit excellent tracking with the SSM/I results. Unlike IWV, however, the CLW statistical uncertainties do not likely reflect the dominant error component in the retrieved trends. The 1992–2005 CLW trend estimates were particularly sensitive to short-term trends in the first and last 2 years of the TMR archive. Additional errors difficult to quantify include strong aliasing effects from precipitation cells and uncertainties in the radiative transfer models utilized in the generation of the TMR CLW algorithm.

Citation: Keihm, S., S. Brown, J. Teixeira, S. Desai, W. Lu, E. Fetzer, C. Ruf, X. Huang, and Y. Yung (2009), Ocean water vapor and cloud liquid water trends from 1992 to 2005 TOPEX Microwave Radiometer data, *J. Geophys. Res.*, *114*, D18101, doi:10.1029/2009JD012145.

1. Introduction

[2] As the dominant greenhouse gas, water vapor plays a central role in the evolution of climate warming induced by the ongoing CO_2 increase. Almost all published climate model results indicate that this role is one of positive feedback [e.g., *Houghton et al.*, 1996; *Schneider et al.*, 1999; *Bony et al.*, 2006; *Soden and Held*, 2006], increasing the sensitivity of surface temperatures to CO_2 buildup by a factor of nearly two [*Held and Soden*, 2000]. In addition, if average relative humidity is largely insensitive to climate change, as suggested by observed correlations of column integrated water vapor (IWV) with sea surface temperature (SST) and troposphere temperature variations [*Wentz and Schabel*, 2000; *Trenberth et al.*, 2005], as well as modeling studies [*Soden et al.*, 2002, 2005], then climate models predict that IWV will increase by 7% per 1°C increase in lower-troposphere air temperature [*Held and Soden*, 2006]. Thus, water vapor trends serve as a surrogate for lower-troposphere temperature changes as well as playing a critical role in determining the total climate effect due to the CO_2 build up. Because tropospheric temperature trends derived from multiplatform instrumentation possess signal

[1]Jet Propulsion Laboratory, California Institute of Technology, Pasadena, California, USA.
[2]Department of Atmospheric, Oceanic and Space Sciences, University of Michigan, Ann Arbor, Michigan, USA.
[3]Division of Geological and Planetary Sciences, California Institute of Technology, Pasadena, California, USA.

0148-0227/09/2009JD012145

to noise several times lower than satellite-derived IWV trends and are inherently more difficult to measure [*Santer et al.*, 2007], the surrogate role may prove to be vital for early detection of the long-term climate signal.

[3] Satellite measurements of column integrated water vapor over the global oceans have been available since the launch of the Scanning Multichannel Microwave Radiometer (SMMR) in 1978 [*Taylor et al.*, 1981]. However, various problems precluded use of the earliest data for reliable measurement of the trends on the decadal time scales required for constraining long-term climate change. First, and foremost, the earlier satellite instruments were not designed to provide long-term operation or sufficiently stable calibration needed for climate change monitoring. Their primary purpose was to provide real time constraints for operational weather prediction models. Over nominal 3–5 year lifetimes problems related to solar heating effects, orbital decay, and instrument degradation contributed to uncertainties in calibration stability at levels too high to allow meaningful extraction of long-term trends. In addition, observations from platforms in different sun-synchronous orbits were subject to diurnal effects, which add to the difficulties of long-term trend extraction. To date, these problems have been addressed most successfully by analyses of data sets from the series of Special Sensor Microwave Imager (SSM/I) instruments flown on six Defense Department Meteorological satellites over the period 1987 to present. The individual instruments have operated over three to five year mission lifetimes with overlap. By careful intercalibration, meaningful IWV decadal trends have been determined over large oceanic regions [*Wentz and Schabel*, 2000; *Wentz et al.*, 2007]. Still, reservations have persisted in the climate modeling community regarding the reliability of trends derived from multiple platform instrumentation [*Soden and Schroeder*, 2000; *Trenberth et al.*, 2006].

[4] The recently completed Ocean Topography Experiment (TOPEX) mission has provided a unique data set for long-term IWV trend measurements, which addresses many of the concerns described above. TOPEX included a support instrument, the TOPEX Microwave Radiometer (TMR), intended to provide wet path delay corrections for the altimeter range measurement. Since wet path delay depends primarily on the column water vapor abundance, the TMR channels (18, 21, 37 GHz) were also near optimum for IWV and cloud liquid water (CLW) measurements. In a recent reprocessing of the entire 1992–2005 TMR data set [*Brown et al.*, 2009], IWV and CLW retrievals have been incorporated into a TMR Climate Data Record (CDR) from which meaningful decadal trend estimates have been extracted and are presented herein.

[5] The advantages of the TMR CDR for identification of global trends are compelling. The TMR instrument was unique with respect to other polar orbiting microwave radiometers in that it obtained a nearly global, complete sampling of the diurnal signal due to its nonsun-synchronous orbit. For the length of the extended mission (1992–2005) a single instrument operated continuously (never turned off, even during mission safeholds) with no significant calibration discontinuities. The TMR operated in a nadir-viewing geometry, limiting polarization effects and providing simpler conversion algorithms for geophysical retrievals. The nadir geometry also eliminated effects of varying emission angle due to orbital decay.

[6] Section 2 of this paper provides a TMR instrument description, including an overview of processing algorithms from antenna temperature through geophysical retrievals. Spatial coverage, resolution, and cycle duration are also described. In section 3 a detailed analysis is provided of the method used to monitor small drifts in the brightness temperature calibrations over the mission lifetime. Arguments are made for the high precision of the calibration drift monitoring which is critical for accurate measurement of the small trends characteristic of long-term climate effects. In section 4 the reprocessing modifications used to generate the TMR CDR are briefly described, followed by a description of the processing used to extract IWV and CLW trends from the 13 year archive. Results for TMR-derived IWV trends are presented in section 5 for global, zonal and regional scales, including a comparison with latitude-dependent SST trends. Comparisons with SSM/I derived IWV trends are made in section 6. TMR-derived CLW trends are presented in section 7 with discussion of the relatively large uncertainties inherent to microwave measurements of cloud liquid. A summary discussion is given in section 8.

2. TMR Instrument Description

[7] The TOPEX Microwave Radiometer (TMR) was a modified version of the SMMR which flew on Seasat and Nimbus-7 [*Njoku et al.*, 1980; *Swanson and Riley*, 1980]. TMR was built almost entirely from spare SMMR flight parts, with modifications which addressed calibration problems encountered by SMMR as well as the specific requirements of the TOPEX mission. The principal modifications included a reduction in channels from five to three, elimination of the SMMR scanning mechanism (TMR was nadir viewing, coaligned with the TOPEX altimeter), and a redesigned multifrequency feed horn (MFFH), which provided higher beam efficiencies to significantly reduce off-earth antenna sidelobe fractions and improve absolute calibration of the brightness temperature measurements. The addition of radomes to the TMR MFFH and sky horn greatly reduced on-orbit radiometer temperature fluctuations, which had been the primary cause of the SMMR calibration problems. More complete temperature cycling in the preflight thermal vacuum tests also provided a significantly improved antenna temperature calibration algorithm for TMR. A detailed description of the TMR hardware, thermal vacuum test modeling, and subsequent antenna temperature algorithm are given by *Ruf et al.* [1995].

[8] As a support instrument, TMR was required only to provide the wet path delay correction to the TOPEX ocean altimetry measurements. Strongly correlated with columnar water vapor (IWV), the wet delay measurements required only three of the original SMMR channels. The 21 GHz channel, on the lower wing of the 22.235 GHz water vapor absorption line, was the primary vapor sensing channel. The 18 and 37 GHz channels provided corrections for the effects of sea surface emissivity variations (due to surface winds) and cloud liquid, respectively. Because of the nadir viewing geometry, polarization effects were minimal, with a small

effect due to wind direction dependency of the sea surface emissivity [*Tran et al.*, 2002]. All three TMR channels operated in a single linear polarization mode throughout the mission. A backup 21 GHz channel with orthogonal polarization was available, but never used in the thirteen years of operation.

[9] The conversion of TMR antenna temperatures to wet path delay involved two additional algorithms. The antenna pattern correction algorithm (APC) deconvolved the effects of the antenna pattern to estimate earth brightness temperatures in the nadir-directed TMR main beams. This algorithm was based on preflight antenna range measurements and modeled estimates of the latitude dependent on-Earth brightness temperatures within the TMR channel sidelobes. Details are provided by *Janssen et al.* [1995]. The geophysical algorithm converted the main beam brightness temperatures to wet path delay using a two step statistical inversion derived from a large radiosonde database. This algorithm, as well as the relationship of wet delay to water vapor, and the effects of clouds and sea winds, is described in detail by *Keihm et al.* [1995]. In-flight verification of the path delay algorithm was demonstrated by comparisons with island radiosonde and ground-based water vapor radiometer measurements [*Ruf et al.*, 1994; *Keihm and Ruf*, 1995].

[10] The TMR main antenna was a partially offset parabolic reflector with projected aperture of 79 cm and half power beam widths of 1.86, 1.56, and 0.98° for the 18, 21, and 37 GHz channels. From the nominal TOPEX spacecraft altitude of 1375 km, this resulted in ground footprint diameters of 43.4, 36.4, and 22.9 km for the three channels. The TOPEX satellite operated in a 9.9 day, nonsun-synchronous exact repeat orbit with an inclination of 66°, providing global sampling over the full range of the local diurnal cycle at all locations every 118.6 days. The nonscanning, nadir-viewing geometry of TMR precludes the more complete coverage provided by scanning instruments such as SSM/I. The average ~30 km TMR footprint samples at the equator are spaced 316 km apart. However, on decade time scales, this grid sample spacing is not expected to significantly impact the derived long-term trends for global and zonal scales.

3. Instrument Drift Correction

[11] The TMR used a cold sky horn and internal ambient reference load to provide in-flight calibration monitoring. The radiometer contained no noise diodes. A ferrite switch directed the radiometer receiver to the calibration targets at 14 s intervals. Because the electrical paths differed between the MFFH, cold sky horn, and ambient reference, any long-term variations in path losses not accounted for in the instrument thermal modeling could have led to calibration drifts which required corrections using external reference sources.

[12] Following the nominal mission phase (3 years) it was recognized that measurements of the lowest radiometer ocean brightness temperatures, under clear, calm, and dry conditions, provided an extremely stable cycle-to-cycle calibration reference. The implementation of this calibration standard for TMR was developed and described by *Ruf* [2000]. It involves generation of cubic polynomial fits to the cumulative distribution function of TMR coldest brightness temperatures for each cycle and each channel, then extrapolation to the zero population values of brightness temperature. This method, referred to as the vicarious cold reference (VCR) algorithm, essentially removes annual signals, and has proven to provide remarkably high stability and precision for monitoring TMR channel drifts over the thirteen year mission lifetime.

[13] Figure 1 shows the 13 year (481 repeat cycles, 9.9 days per cycle) history of the TMR channels' VCR-derived coldest brightness temperatures, plotted as variations from the cycle one values. In addition to the VCR, stable, densely vegetated regions in the Amazon rain forest were used to monitor the calibration at the hot end of the TMR dynamic range [*Brown and Ruf*, 2005; *Brown et al.*, 2009]. There were no observed trends in the hottest TMR brightness temperatures, suggesting that the calibration drifts were due to an instrument gain drift and required an appropriate correction that scales to zero at the hottest end. As will be demonstrated, the drifts shown are due to instrument effects and can be accurately removed prior to determination of the long-term climate-induced variations. The largest drift, averaging ~0.27 K/a during the first 6 years of the 18 GHz channel data, was first suggested from deduced ~2 mm/a drifts in the comparison of sea level measurements between TOPEX and the global tide gauge network [*Mitchum*, 1998]. The latitudinal dependence of the relative drift suggested that a drift in the TMR wet delay correction be considered as an explanation. As it turned out, the global average 2 mm/a drift seen in the tide gauge sea level comparisons was equivalent in sense and magnitude to the wet delay drift predicted by the 18 GHz brightness temperature (TB) drift derived from the VCR algorithm [*Keihm et al.*, 2000]. This result provided confidence that the later smaller drifts seen in the VCR records of the 21 and 37 GHz channels were true instrument effects which could be removed in the reprocessing for the climate data record.

[14] The above analysis of TMR instrument drift measurement relies on the assumption of long-term stability of the vicarious cold reference in the presence of climate perturbations. It is imperative that potential drifts in the VCR TBs due to actual climate changes not be mistaken for instrument drifts and removed from the atmospheric trend record. To demonstrate that is not the case, we consider the following argument.

[15] The argument can be summarized by recognizing that the coldest brightness temperatures observed over the ocean between 18 and 37 GHz are not tied to a climate minimum (e.g., coldest SST or driest atmosphere) but occur because of a minimum in the sea surface brightness that occurs in the middle of the climatic distribution of SSTs. Over the range 18–37 GHz, the minimum surface emission from the Earth occurs for a flat ocean surface at a frequency-dependent optimal SST where the product of the sea surface emissivity and sea surface temperature is minimum. This optimum SST is 15.1°C at 18.0 GHz, 17.9°C at 21.0 GHz and 26.4°C at 37.0 GHz [*Ruf*, 2000]. The surface emission is then propagated through the atmosphere where oxygen, water vapor and liquid water drops absorb and reemit the radiation, serving to increase the top of atmosphere (TOA) TB. For a globally distributed TB data set, water vapor and SST will be the most dominate geophysical variables in driving the probability of the coldest TMR TBs. Because

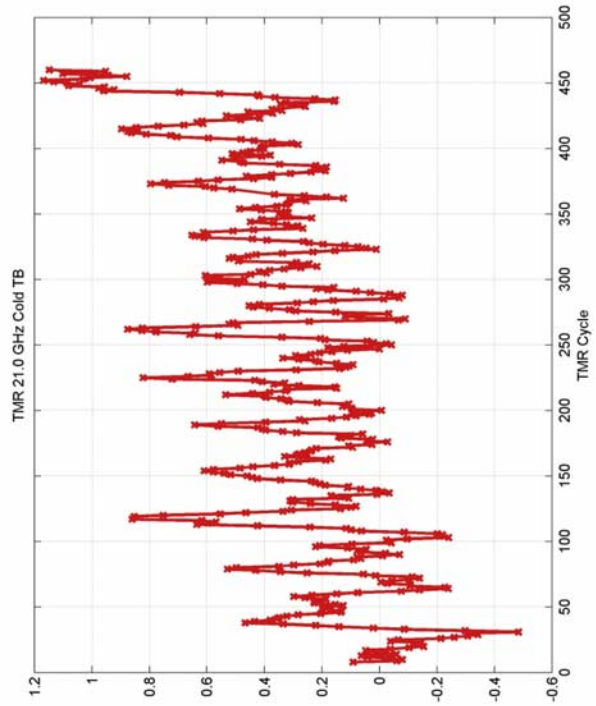

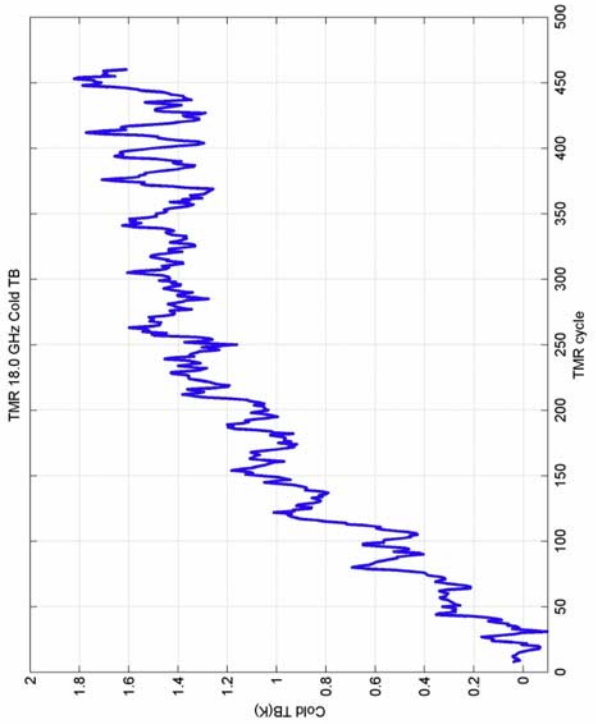

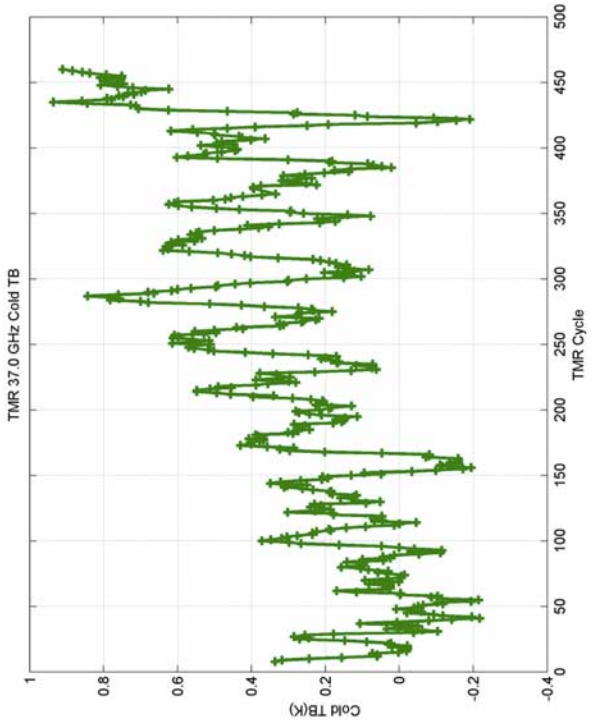

Figure 1. Thirteen year history of the three TMR channels' VCR-derived coldest brightness temperatures plotted as variations from cycle one values.

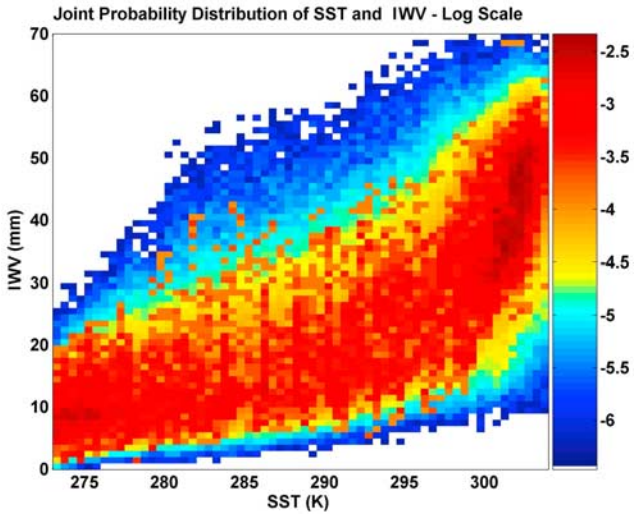

Figure 2. Joint probability distribution of sea surface temperature and IWV computed from the NCEP/NCAR 4*x* daily fields for 1998.

water vapor and SST are inherently coupled through the Clausius-Clapeyron relationship, the coldest TOA brightness temperatures will occur over a range of SST and IWV combinations near the emission optimal SST. In general, as the surface temperature decreases, the integrated water vapor decreases. As we move away from the SST of minimum surface emission toward colder SSTs, the probability of drier atmospheric conditions increases, creating a balance between the increasing surface contribution and the decreasing atmospheric contribution. This offsetting effect broadens the probability distribution function of the coldest TOA TBs in geophysical state space, which in turn desensitizes the VCR to climate variability.

[16] To examine this further, a large database of modeled brightness temperatures at the TMR frequencies was generated using National Centers for Environmental Prediction (NCEP)/National Center for Atmospheric Research (NCAR) reanalysis 4*x* daily fields [*Kistler et al.*, 2001] for 1998. Figure 2 shows on a logarithmic color scale the joint probability distribution of SST and integrated water vapor computed from the NCEP database. It is observed that dry atmospheric conditions occur over a wide range of SST values.

[17] Statistical box plots were next generated from the modeled TB database to illustrate the distribution of 18.0, 21.0 and 37.0 GHz TOA TB with respect to SST and IWV (Figure 3). The box plots show the TB median (horizontal red line in box), quartiles Q1 and Q3 (lower and upper box boundaries), and the data extremes for each of the three channels, computed separately for binned values of IWV (Figure 3 (top)) and SST (Figure 3 (bottom)). The upper- and lowermost data in red indicates outliers defined as points lying 1.5 × (Q3−Q1) above or below the quartile values. The arrows on Figure 3 (bottom) indicate approximately where the minimum surface emission occurs.

[18] It is indeed observed from the box plots that the coldest brightness temperatures at each frequency are observed over a broad range of SST and IWV combinations particularly for the 18 and 37 GHz channels. The 21 GHz cold TBs occur toward the dry end of the spectrum, yet still span an IWV range of 0–4 mm, nearly ten times the measured values for decadal variability (see section 4). Thus the cold TB reference is not linked to a climatic minimum (coldest temperature or driest air column), but to a range of possible geophysical states away from the edge of the probability distribution. In this way, the cold reference will be less sensitive to global climate change because it won't shift even if the climatic minimum shifts. To bias the cold reference on long time scales, the probability of every combination of SST and IWV which lead to the coldest TOA TBs would have to simultaneously decrease below some threshold. This is a highly unlikely scenario for global climate change. We contend that the variations in the VCR-derived coldest TMR brightness temperatures shown in Figure 1 are due entirely to instrument induced drifts which can be removed prior to climate trend analyses.

4. TMR Climatology Data Record and Trend Computations

[19] Following the end of the TOPEX mission in 2005, efforts were begun to produce a revised Geophysical Data Record (GDR) for the entire mission, incorporating correction algorithms for systematic calibration errors detected from analysis of the original GDR. For the TMR, this offered the opportunity to produce an auxiliary data record, including climate parameters such as integrated water vapor and cloud liquid. The post mission TMR Climate Data Record (CDR) [*Brown et al.*, 2009] incorporated three significant processing modifications. The first was the removal of the instrument-induced TB trends described in section 3. This was accomplished by generating third order fits to the VCR data of Figure 1, including a linear scaling with TB level. An error analysis showed that uncorrelated 20% errors in the instrument channel TB drift corrections would result in a ∼0.3% error in derived IWV trends, equivalent to the statistical uncertainty of the trend measurements. If the channel drift correction errors were correlated between channels, the resulting IWV trend error would be less.

[20] The second modification was a revision of the model for earth sidelobe brightness temperatures required for the APC algorithm. In the original algorithm, on-Earth sidelobe contributions were estimated from TMR beam data, island radiosonde data, and a mean Earth TB model with a simple latitude dependence [*Janssen et al.*, 1995]. In the revised algorithm on-Earth sidelobe TBs are computed from 1 × 1° earth maps on the basis of seasonal averages of actual TMR TB measurements obtained over the entire mission, including data over land. This improvement to the APC algorithm was suggested by *Obligis et al.* [2007].

[21] The third processing modification for the TMR CDR was the conversion of the wet path delay retrieval algorithm to one for IWV using radiosonde-derived statistics. A similar two step stratification scheme was used as for the wet delay algorithm described by *Keihm et al.* [1995]. The IWV algorithm uses a log linear combination of the brightness temperatures of the form

$$\mathrm{IWV} = c_0(\mathrm{WS}_0, \mathrm{IWV}_0) + \sum_f c_f(\mathrm{WS}_0, \mathrm{IWV}_0)\log(280 - T_B(f)), \quad (1)$$

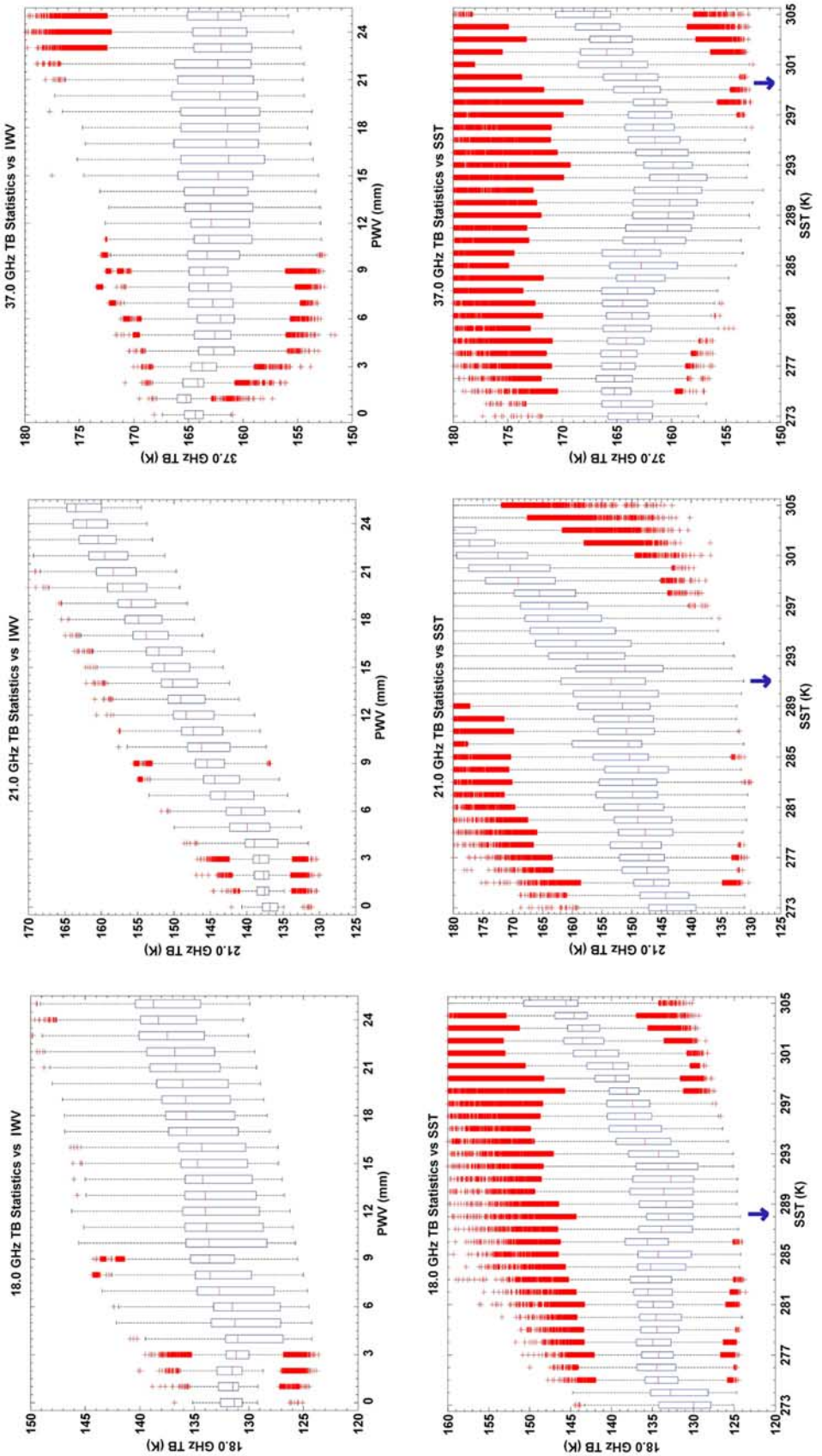

Figure 3. Statistical box plots of model TB binned by (bottom) SST and (top) IWV for (left) 18, (middle) 21, and (right) 37 GHz channels.

where the retrieval coefficients (provided by *Brown et al.* [2009]) are generated from a large database of modeled brightness temperatures from island radiosonde data. To account for small nonlinearities in the algorithm, the retrieval coefficients c_0 and c_f in (1) are stratified by wind speed and IWV range and interpolated by the algorithm to a first guess IWV and wind speed. In (1), IWV is the final retrieved integrated water vapor value and WS_0 and IWV_0 are the first guess wind speed and integrated vapor values computed from a global algorithm. The summation over f refers to the three TMR channels.

[22] It is important to note that the accuracy of the long-term IWV trend results presented in section 5 is largely dependent on the validity of the instrument TB drift correction. The APC and retrieval algorithm modifications do not significantly affect decadal trend results on global and large regional scales. Further details of the algorithm modifications and instrument drift corrections utilized in the CDR production are provided by *Brown et al.* [2009].

[23] The cloud liquid water retrieval algorithm is a polynomial combination of the TMR brightness temperatures

$$\mathrm{CLW} = b_0 + b_1 T_B(18.0) + b_2 T_B(21.0) + b_3 T_B(37.0) + b_4 T_B(37.0)^2, \quad (2)$$

where $b_0 = 4345$, $b_1 = -20.12$, $b_2 = -1.64$, $b_3 = -38.29$, and $b_4 = 0.185$. Computed CLW values less than zero are converted to zero (clear conditions) in the processing. Equation (2) is identical to the CLW algorithm used in the final TOPEX Geophysical Data Record processing to account for the small component of path delay due to suspended cloud liquid. It was derived by statistical correlation from the same island radiosonde database used for the IWV algorithm. Because CLW is not measured directly by radiosondes we employed a cloud model based on the concept that the liquid water density at any level within a cloud is proportional to the absolute humidity difference relative to the cloud base [*Fletcher*, 1962]. We used a proportionality factor of 0.5, consistent with aircraft in situ measurements [*Malkevich et al.*, 1981]. We defined the cloud boundaries as occurring where the relative humidity crosses 94%, a value somewhat arbitrary but sufficient to allow generation of a globally representative range of CLW conditions. No attempt was made to correct for precipitation effects. The implications for absolute and trend accuracy of TMR-derived CLW are discussed in section 7.

[24] The generation of long-term trend information from the TMR CDR proceeded as follows. First, the CDR archive was filtered to eliminate land, sea ice, and heavy precipitation data (see below). Global ocean regions were then divided into $2.5 \times 2.5^\circ$ grid boxes. The 2.5° size ensured that each grid box would be sampled at least once per cycle. Next, all unfiltered 1 s measurements of IWV and CLW in each grid box were averaged over each 10 day cycle. Finally, global and hemisphere cycle averages were generated by applying cos(latitude) weighting to all appropriate grid boxes. This averaging method ensures that each latitude range is properly weighted with the effects of latitude-dependent landmass fraction eliminated. After generation of the entire 481 cycle archive, the mean seasonal cycle was removed by subtracting the appropriate monthly mean of the entire 13 year data set for all data in each zone of interest. Trends for IWV and CLW were then computed for each zone using linear least square fits. Uncertainties of the slope parameters were also computed including corrections for lag 1 autocorrelation [*Santer et al.*, 2000].

[25] Potential aliasing of diurnal signals into the trend results were also evaluated. The full TMR data set was used to compute the diurnal variations of both cloud liquid water and integrated water vapor. The diurnal signal of CLW was found to have a peak-to-peak magnitude of 15 g/m^2. The diurnal water vapor signal was much weaker with a peak-to-peak magnitude of 0.5 mm. The sampling of TOPEX was such that the diurnal cycle was fully sampled approximately 3 times per year. It was found that diurnal signals would be aliased into the regional and global time series with this period, but the impact on the trend when computed over several years was negligible.

[26] All reported trends were derived after filtering out all 1 s CLW retrievals >1000 g/m^2. Values of CLW >1000 g/m^2 are generally indicative of heavy rain in all or a large fraction of the TMR footprint. These data are excluded because TMR CLW retrieval accuracies are reduced in the presence of precipitation because of scattering and the differing emission spectra of raindrops. In repeating the processing using other rain flag filters the IWV trend fits were found to be insensitive to the CLW rain flag threshold. The CLW trends were not (see section 7).

5. Thirteen Year IWV Results From TMR

5.1. Global and Latitude-Dependent Trends

[27] Figures 4a–4c show the TMR-derived thirteen year histories of cycle averaged IWV for the global (60°S–60°N), Northern Hemisphere (NH, 0–60°N) and Southern Hemisphere (SH, 0–60°S) zones after removal of the seasonal signals. Positive signatures from the 1998 El Nino event are clearly present in the global and SH data sets. The fitted linear trend slopes are shown, both in mm and fraction (percent) of the mean values. The uncertainty levels represent ±1 standard deviation of the slope parameters corrected for autocorrelation of the cycle-averaged data. The lag 1 autocorrelation for the global IWV trends is relatively high, 0.6, indicating that the stated slope error of 0.38% represents a doubling of the uncorrected 1σ error. Lag 1 autocorrelation values for the hemisphere IWV trends are smaller, 0.1 (northern) and 0.3 (southern). However, the statistical uncertainties do not reflect the sensitivity of the derived trends to global scale transient events such as El Nino and volcanic eruptions. The occurrence of the large 1998 El Nino signature near the middle of the IWV anomaly time series has minimal effect on the decadal trend estimate. In contrast, the Mt. Pinatubo eruption occurred in June of 1991, with subsequent decreases in global tropospheric temperatures and water vapor which lasted 2–3 years [*Harries and Futyan*, 2006]. The negative effect was partially offset by a mild El Nino period in 1992. Unfortunately, the maximum Pinatubo effect coincided with the beginning of the TMR archive where the effect on slope computations is most enhanced. The effect was evaluated by computing trend values using only the 1995–2005 archive. The result indicated a reduction of the TMR-derived global

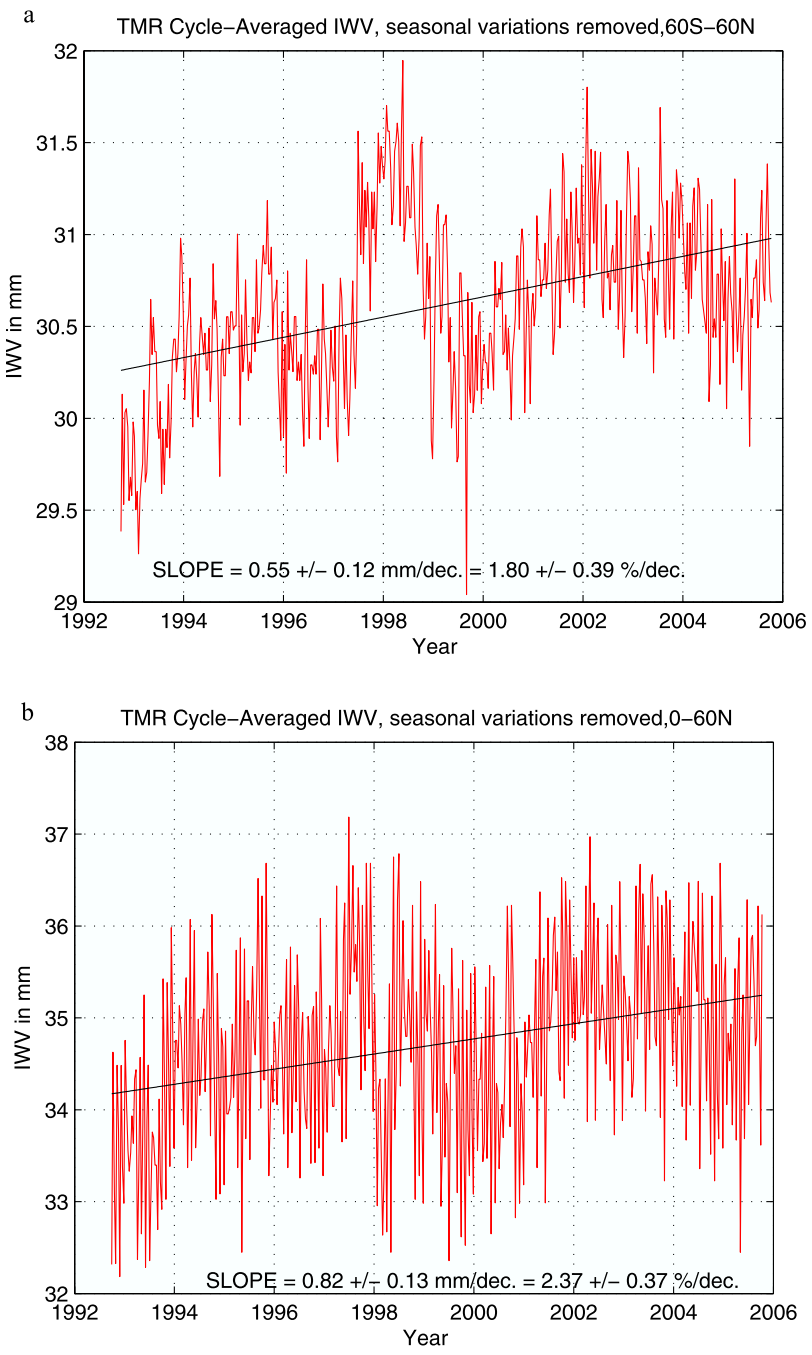

Figure 4. TMR-derived 13 year histories of cycle averaged IWV for global and hemisphere zones after removal of the mean and annual signals for (a) 60°S–60°N, (b) 0–60°N, and (c) 0–60°S.

IWV trend to 1.0%/decade. In contrast, removal of the last two years of the archive resulted in an increase in the derived global IWV trend to 2.4%/decade. These results clearly illustrate the sensitivity of derived decade-scale trends to archive length and the placement of transient events in the time series.

[28] Taken at face value, the global IWV trend result of 1.8%/decade strongly supports previous trend estimates on the basis of the SSM/I archive, i.e, 1.8%/decade from 1987 to 1998 SSM/I data [*Wentz and Schabel*, 2000], 1.3%/decade from 1988 to 2003 SSM/I data [*Trenberth et al.*, 2005], 1.4%/decade from 1988 to 2005 SSM/I data [*Soden et al.*, 2005], and 1.3%/decade from 1988 to 2006 SSM/I data [*Wentz et al.*, 2007]. The TMR-derived hemisphere contrast in IWV trend (2.4%/decade in the NH versus 1.0%/decade in the SH) also supports the approximately 2:1 trend ratio estimated by *Wentz and Schabel* [2000]. This observed agreement of decadal scale IWV trends derived from two independent satellite data archives provides needed confidence that long-term climate trends can be reliably measured by current state-of-the-art satellite microwave radiometers. In particular, the single instrument TMR results largely validate the creative intercalibration methodologies required to pro-

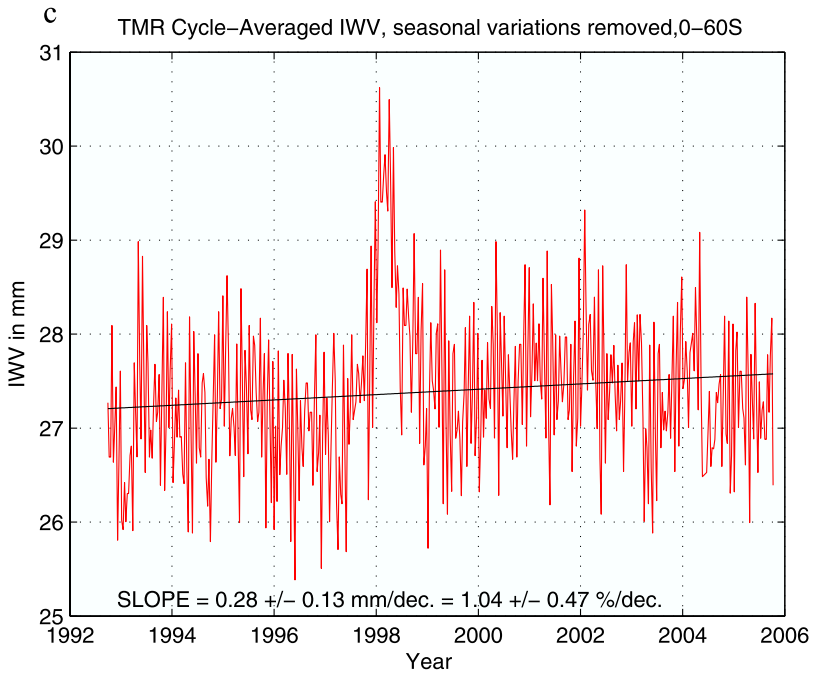

Figure 4. (continued)

duce meaningful decadal scale trends from the multiplatform series of SSM/I instruments.

[29] In addition to the global and hemispheric analyses, the TMR archive has been processed to reveal latitude-dependent IWV trends as shown in Figure 5. Trend values are shown for each 5° latitude band from 60°S to 60°N. The red traces indicate the 1σ error limits after autocorrelation adjustment. Standing out are the hemisphere trend peaks at the 3–4%/decade levels near 40°N and 40°S and the sharp trend minimum in the southern tropical ocean centered at 10°S. A comparison of interest is provided by the latitude dependence of SST trends, derived from the Goddard Institute for Space Studies (GISS) database (http://data.giss.nasa.gov/gistemp/maps/) for the 1992–2005 interval, and shown as the black trace in Figure 6. The red trace is derived from the TMR-based IWV trend data shown in Figure 5 assuming an IWV/SST trend correlation of 7%/K, the scaling predicted for IWV/air temperature with the constant relative humidity assumption. The green trace is derived from the TMR IWV trends by assuming an 11%/K

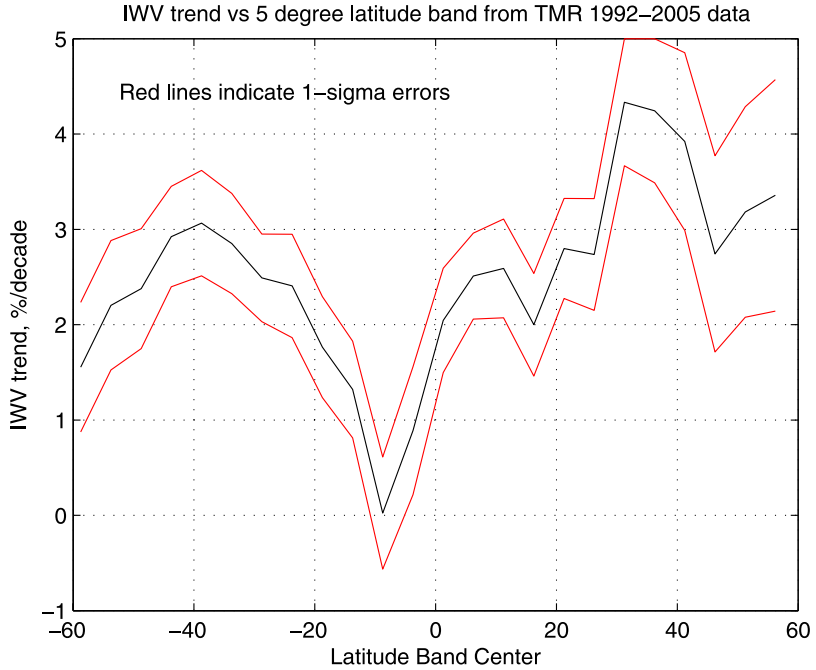

Figure 5. Latitude dependence of TMR-derived IWV trends. Red traces indicate 1σ error limits.

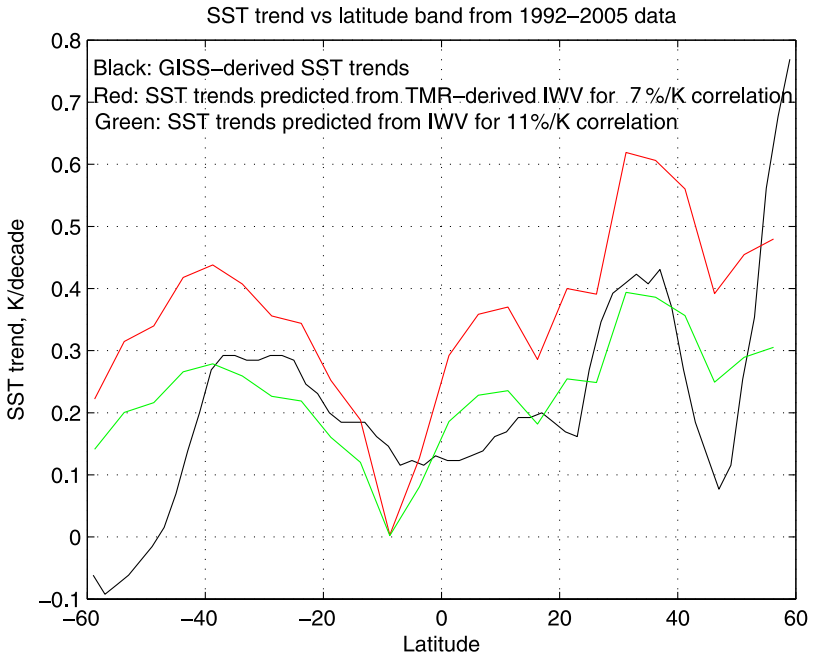

Figure 6. Latitude dependence of 1992–2005 SST trends from GISS. The red and green traces are the conversions from the TMR trends of Figure 5 using 7 and 11%/K scaling, respectively. The better fitting 11%/K model is consistent with a constant relative humidity model when the expected amplification of air temperature variations relative to SST is taken into account.

correlation, consistent with midlatitude radiosonde observations of the seasonal variations in IWV and surface temperature as noted by *Wentz and Schabel* [2000]. The 11%/K scaling between IWV and SST trends holds up well in the 40°S–40°N latitude region, consistent with seasonal correlations observed in satellite data of the tropical oceans [*Aumann et al.*, 2007]. Note that an IWV/SST trend scaling >7%/K does not necessarily invalidate the constant relative humidity model. With a moist adiabatic lapse rate it is expected that tropospheric temperature variations will be amplified relative to SST [*Trenberth et al.*, 2005]. The amplification effect is supported by the TMR results as well as previous trend comparisons based on SSM/I data [*Wentz and Schabel*, 2000; *Trenberth et al.*, 2005].

5.2. Regional Trends

[30] Regional IWV trends, shown in the global maps in Figure 7a for 2.5 × 2.5° pixels, reveal a much more complex picture with greater variability, ranging over trend values of ∼±8%/decade. Although the statistical uncertainties in the trend fits for individual pixels are much larger than the zonal values, the regional variations are sufficient to warrant speculative interpretation. When compared with the regional variations in SST trends derived from the NASA GISS site for the same period (Figure 7b), it is clear that for the regions where the IWV and SST trends are more significant, the relation between IWV and SST follows an approximate Clausius_Clapeyron relation (i.e., an IWV increase of about 7–10% per Kelvin of SST). There are also smaller regions, generally of smaller trend signals, where the IWV and SST trends show little or negative correlation. These regions may be affected by relative lags in the IWV and SST response or natural decadal scale variability.

[31] Of particular interest is the Eastern Pacific with clear negative IWV trends dominant off the coasts of North and South America. These negative trends, as well as the negative SST trends in these two regions, are consistent with a decrease in the depth of the boundary layer, a consequent increase in the frequency of stratocumulus regimes (shallow boundary layers with large cloud cover), and a decrease in the frequency of cumulus regimes (deeper boundary layers and more intermittent clouds). In addition, in other regions of the midlatitudes and the subtropics, the TMR results show positive trends in IWV. As described above, the more significant regions with positive IWV trends correlate with positive SST trends and are also consistent with having larger IWV in deeper boundary layers which are in turn associated with cumulus clouds rather than larger sheets of stratus or stratocumulus clouds.

6. Comparisons With SSM/I 1992–2005

[32] A comparable ocean IWV data set, in terms of quality and long-term operation, is the SSM/I data record, which has been sewn together through the careful intercalibration of multiple satellites. Despite the uncertainties associated with deriving decadal trends from instruments on multiple platforms, the SSM/I data set is generally considered the best long-term record of IWV trends to date [*Wentz and Schabel*, 2000; *Trenberth et al.*, 2005]. Because the TMR brightness temperature calibration and IWV retrieval algorithm are largely independent of SSM/I, demonstrated consistency between TMR- and SSM/I-derived IWV trends should greatly contribute to the confidence in these trend estimates for climate applications.

[33] TMR-predicted IWV trends were compared to those by SSM/I based on SSM/I version 6 IWV data acquired

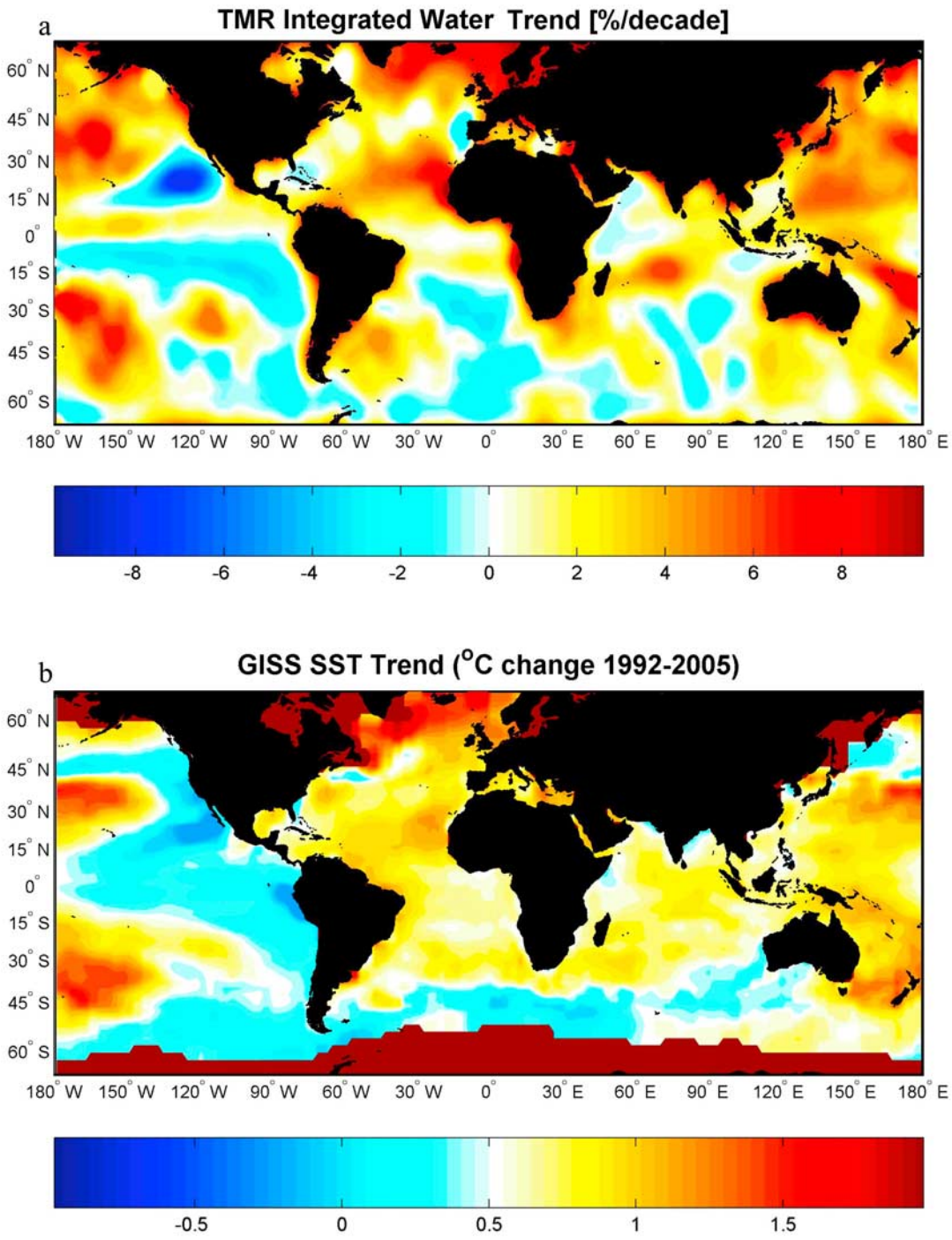

Figure 7. (a) TMR-derived regional trends of IWV over 2.5 × 2.5° ocean pixels in %/decade. (b) SST regional trends derived from GISS website data over the 1992–2005 interval.

from Remote Sensing Systems. Figure 8 shows the 1992–2005 IWV averages for the tropics (20°S–20°N) from both TMR and SSM/I data. The data from all instruments (one TMR, five SSM/I) were smoothed using 90 day averages. The 1 mm (~2.4%) offset between the two data sets is at the level one would expect from retrieval algorithm modeling differences. Note, however, the extremely consistent tracking of both the seasonal and interannual variations. Tracking of the seasonal variations (and the 1998 El Nino event) demonstrates a precision of 0.1–0.2 mm between the two instruments. With removal of the mean and annual components a long-term trend of 0.8 mm/decade (1.8%/decade) is computed for both data sets. Note also in Figure 8 an apparent increase in the upward trend rate following the 1998 El Nino event.

[34] On a global scale, Figure 9 shows time series of the global ocean average (60°S–60°N) TMR-SSM/I IWV difference at crossover points for both morning and evening SSM/I passes. Crossover points are defined as points for which both TMR and SSM/I data exist with less than 25 km

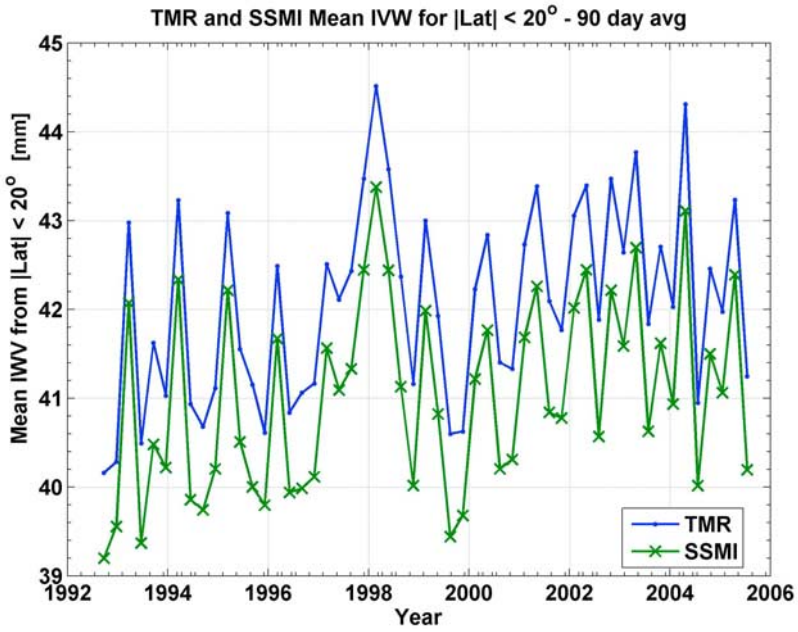

Figure 8. Time series of 90 day averaged IWV in the tropical zone (20°S–20°N) derived from both the SSM/I and TMR data. Note the precision of tracking between instruments on both seasonal and decadal time scales.

spatial and 1 h temporal separation. Five different SSM/I units, identified by color, are included in the Figure 9 comparison covering the period September 1992–2005. A remarkable consistency is observed between the TMR and each SSM/I time series, pointing to the quality of the SSM/I intercalibration and the TMR long-term calibration. The global bias between TMR and SSM/I is about −0.6 mm (∼2% of the mean global IWV signal) and is stable to ∼0.05 mm between the SSM/I units. There is also observed a consistent offset in the difference of ∼0.04 mm between the SSM/I morning and evening passes. Most importantly, the relative drift between TMR and SSM/I IWV is less than 0.1 mm/decade, a factor of 5–6 less than the independently measured TMR- and SSM/I-derived trends. These results, produced by two independent radiometer systems, provide compelling evidence that satellite microwave instruments

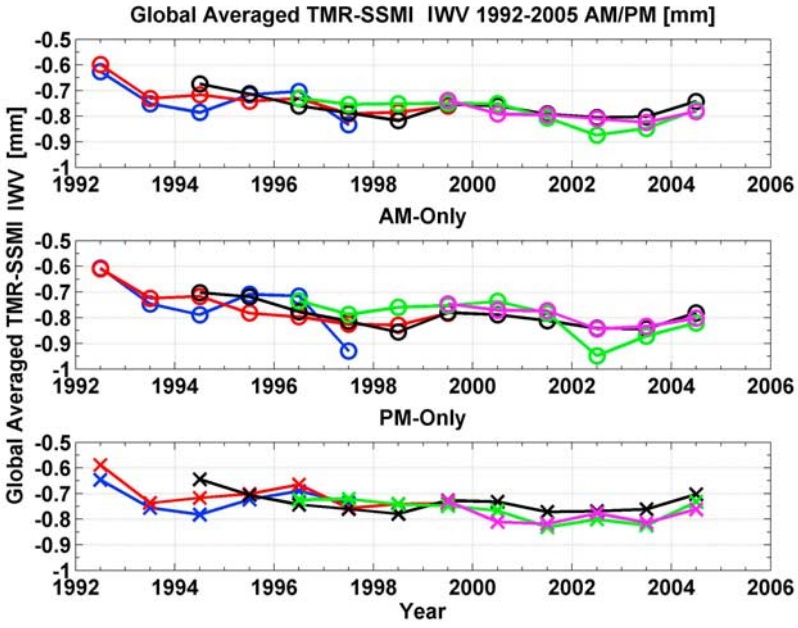

Figure 9. Time series of the global ocean (60°S–60°N) average TMR-SSM/I IWV difference at crossover points for both morning and evening SSM/I passes. Note the consistency between the five different SSM/I units (differentiated by color) covering the 1992–2005 period.

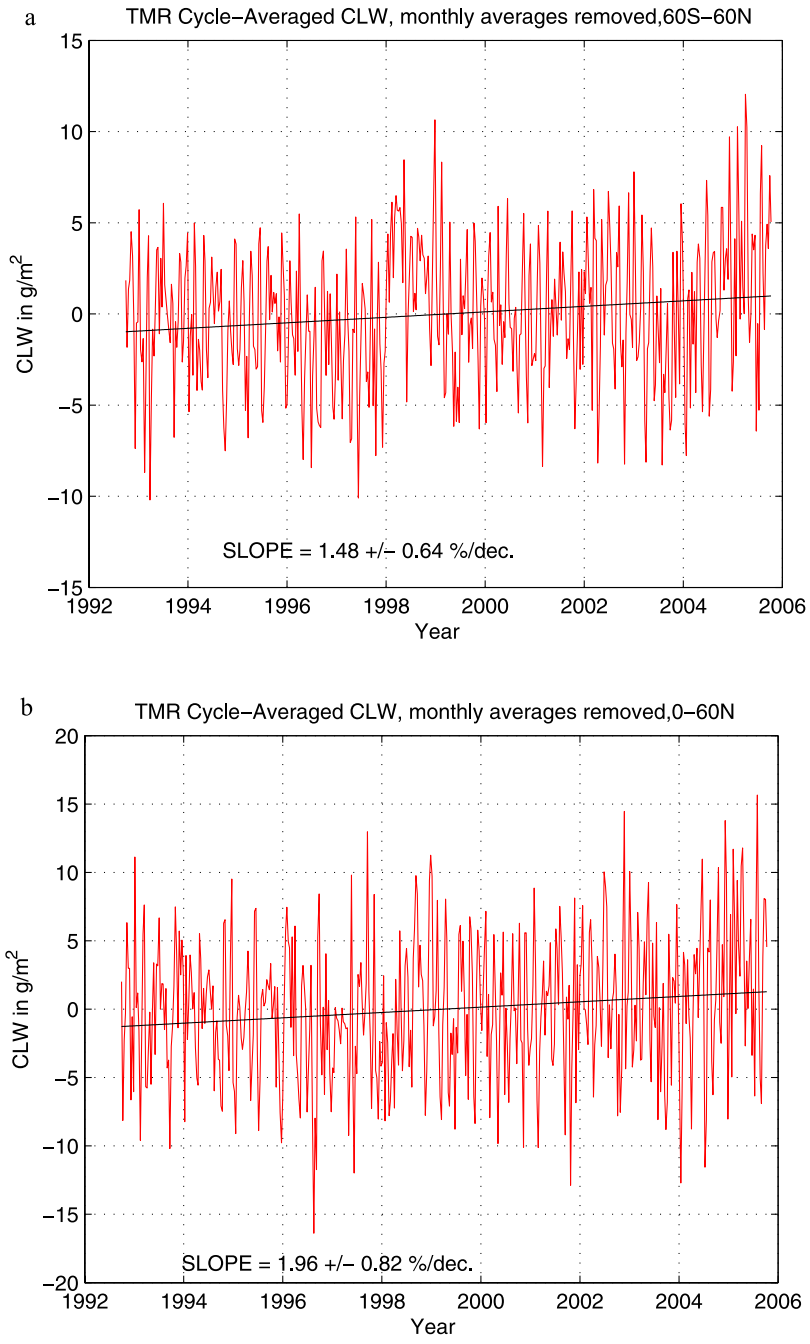

Figure 10. TMR-derived 13 year histories of cycle averaged CLW for global and hemisphere zones after removal of the mean and annual signals for (a) 60°S–60°N, (b) 0–60°N, and (c) 0–60°S.

can provide meaningful decadal trends in overocean water vapor abundance.

7. TMR-Derived CLW Trends

[35] The TMR-derived CLW global and hemisphere trends are shown in Figures 10a–10c. The statistical uncertainties indicate that the measured CLW trends are only marginally significant at the 95% (two sigma) confidence level, but the results are noteworthy in their comparison with the derived IWV trends: 1.5%/decade CLW, 1.8%/decade IWV for 60°S–60°N; 2.0%/decade CLW, 2.4%/decade IWV for 0–60°N; 1.1%/decade CLW, 1.0%/decade IWV for 0–60°S. Within the statistical uncertainties, the TMR results suggest that the large-scale IWV and CLW fractional trends are essentially equal. However, this result may be largely fortuitous. The TMR CLW trend results are very sensitive to steeper, shorter-term trends near the end points of the archive. For example, removal of the upturned data in the last two years of the archive reduces the derived global and hemisphere CLW trends by half or more. It is also widely recognized that satellite microwave retrievals of suspended cloud liquid are subject to systematic errors which could easily exceed the formal statistical uncertain-

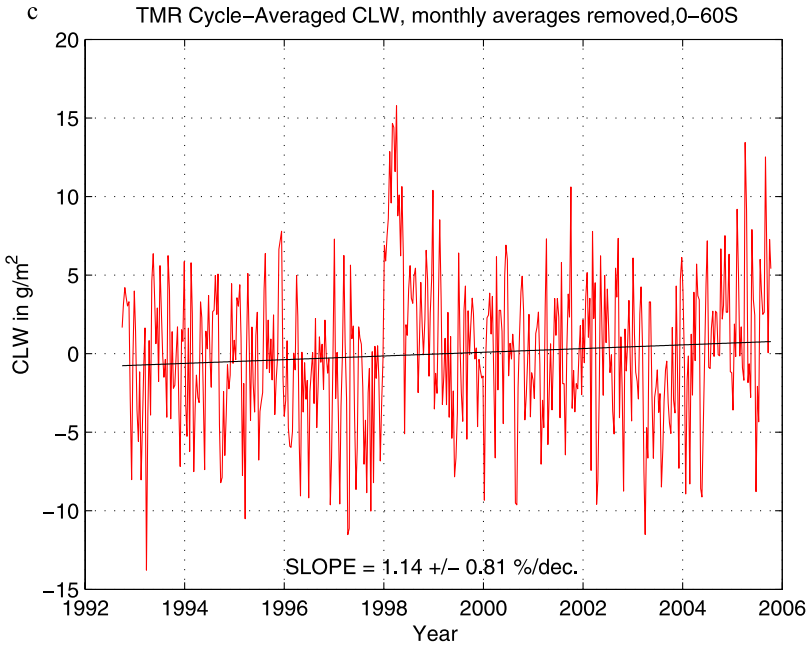

Figure 10. (continued)

ties. The satellite cloud liquid trends are less robust than the IWV measurements, being sensitive to differences in cloud formation and precipitation processes as well as the difficulties of separating the effects of clouds, rain, and wind on microwave brightness temperature signals [*Lin and Rossow*, 1994; *Stephens and Kummerow*, 2007]. Especially important is the presence of precipitation cells in the radiometer footprint, which will strongly mimic CLW signatures in the brightness temperature measurements. The precipitation effects are made apparent when the CLW trends are recalculated with higher rain threshold filters. When no rain threshold filter is applied (all retrieved CLW values included) the global and hemisphere CLW trends increase by ∼20%, suggesting that a positive precipitation trend for large-scale storms may be present. This result is consistent with the positive global precipitation trend derived from SSM/I retrievals [*Wentz et al.*, 2007]. In addition to the precipitation uncertainty, aliasing (cross talk) effects on CLW retrievals due to long-term variations in water vapor, wind speed, and sea surface temperature must also be assessed.

[36] To assess the validity of the TMR-derived CLW archive we first compared the 1992–2005 time series with a CLW data set (University of Wisconsin Climatology Record [*O'Dell et al.*, 2008]) derived from SSM/I data using a much more sophisticated retrieval algorithm [*Hilburn and Wentz*, 2008] developed by Remote Sensing Systems (RSS). On global scales it was immediately observed that TMR-derived mean levels of CLW were ∼50% higher than those from the RSS algorithm. This was not unexpected in that the RSS algorithm includes a correction for precipitation when flagged. The TMR algorithm overestimates global levels of CLW due to the precipitation effects. The high average bias is also likely due to the selection of 94% relative humidity as the indicator of cloud boundaries in radiosonde data used to generate the TMR CLW algorithm (see section 4) and the fact that negative retrievals (clear conditions) are set to zero in that algorithm. For the purpose of comparing CLW variations produced by the RSS and TMR algorithms, we scaled the TMR retrievals by the ratio of the SSM/I/TMR mean CLW values over the 1992–2005 interval. The results for the tropics, expressed as time series of averages for the 30°S–30°N latitude band, are shown in Figure 11. The data labeled SSM/I are 1 month averages taken from Figure 1 of *O'Dell et al.* [2008]. The TMR data are 3-cycle (∼30 day) running averages. The high level of seasonal scale tracking of the two data sets provides evidence that the retrieved TMR CLW variations are indicative of real climate effects, but by itself does not necessarily validate the much smaller variations derived for decadal time scales.

[37] To assess potential systematic errors in the TMR-derived CLW trends due to aliasing, it is instructive to examine the trend in the brightness temperature record of the 37 GHz channel, the primary cloud liquid channel which is three times more sensitive to column liquid water variations than either the 18 or 21 GHz channels. Figure 12 shows the TMR global average 1992–2005 record and fitted TB37 trend after the VCR correction. The clear positive trend, 0.45 K/decade, is statistically significant well within the 95% (2σ) confidence level. This trend is driven by global average changes in all or some of the forcing atmospheric and ocean surface properties: IWV, CLW, precipitation, SST, and wind speed (WS). The question to be addressed is what combination of these parameter trends is consistent with the measured TB37 trend. The possibilities are explored by examining the sensitivity of TB37 variations to forcing parameter variations

$$dT_B37/dt = (\partial T_B37/\partial \mathrm{IWV})d\mathrm{IWV}/dt + (\partial T_B37/\partial \mathrm{CLW})d\mathrm{CLW}/dt + (\partial T_B37/\partial \mathrm{WS})d\mathrm{WS}/dt + (\partial T_B37/\partial \mathrm{SST})d\mathrm{SST}/dt. \quad (3)$$

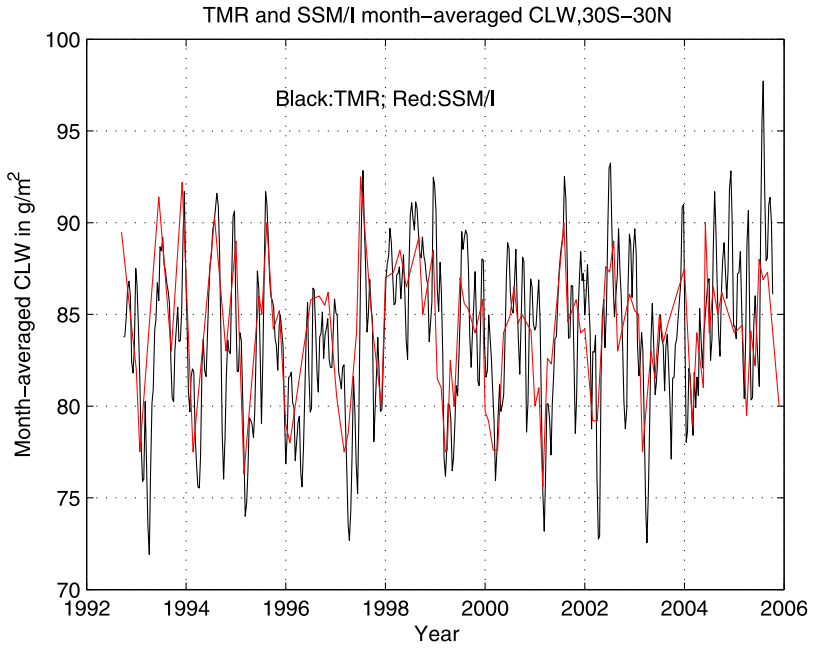

Figure 11. Time series comparison of SSM/I and TMR derived CLW for the tropics. The TMR-derived CLW values have been scaled to the SSM/I mean.

We assess the implications of equation (3) assuming that the sensitivities to the parameters are constants; i.e., nonlinear effects are ignored. The parameter derivatives were calculated at global mean values of IWV, WS, and SST, and for a 500 m thick cloud at 4 km height containing 200 g/m^2 of suspended liquid. The resultant 37 GHz nadir brightness temperature dependencies are well constrained at the 10–20% accuracy level based on experiments [e.g., *Wilheit*, 1979] and modeling studies [e.g., *Keihm et al.*, 1995], and are given as follows:

$$\partial T_B 37/\partial \mathrm{IWV} = 0.53\ \mathrm{K/mm},$$

$$\partial T_B 37/\partial \mathrm{CLW} = 0.066\ \mathrm{K/gm^{-2}},$$

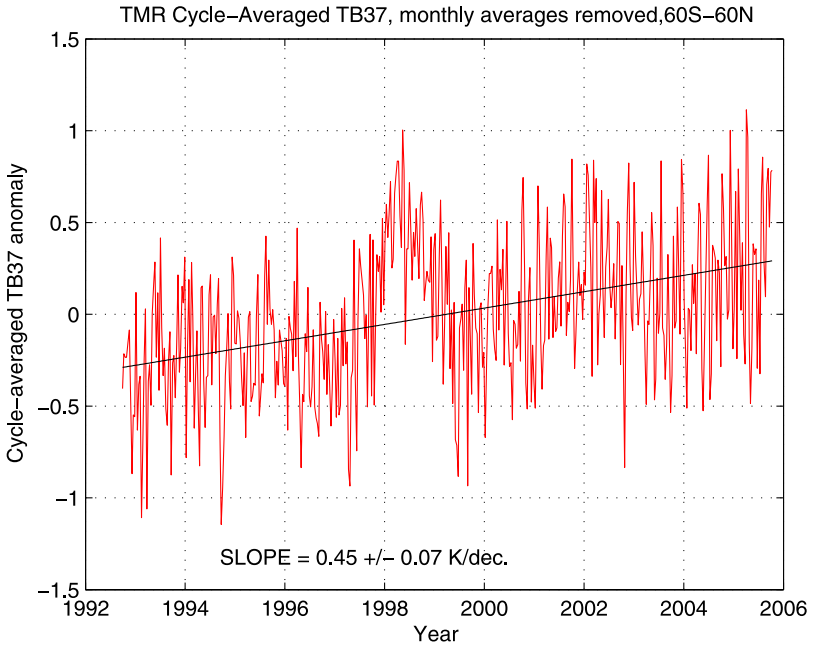

Figure 12. Time series of TMR 37 GHz brightness temperature anomalies with slope.

$$\partial T_B 37/\partial \mathrm{WS} = 1.0\ \mathrm{K/m/s}\ (\text{for WS} > 7\ \mathrm{m/s}),$$

$$\partial T_B 37/\partial \mathrm{SST} = 0.$$

The zero dependence on SST derives from the inverse relation between emissivity and SST at 37 GHz. The 10–20% uncertainties in the IWV and CLW dependencies derive partially from nonlinear effects, absorption model uncertainties, and the effects of height distribution and cloud temperature. Using the above values in equation (3) and our retrieved values of global IWV and CLW trends we get

$$\begin{aligned} dT_B 37/dt &= 0.53(0.55) + 0.066(2.26) + d\mathrm{WS}/dt \\ &= 0.29 + 0.15 + d\mathrm{WS}/dt \\ &= 0.45\ \mathrm{K/decade(measured)}, \end{aligned}$$

indicating that the TB37 trend can be essentially explained by the derived IWV and CLW trends only. This result, while supportive of the derived IWV and CLW trends, does not exclude other interpretations of the TB37 trend result. It is noteworthy that long-term trends in the SSM/I measurements are consistent with 0.8%/decade and 1.4%/decade increases in global surface winds and precipitation [*Wentz et al.*, 2007] as well as no discernible trend in cloud liquid [*O'Dell et al.*, 2008]. The 37 GHz TMR TB trend is also consistent with those results. The key argument is that only about 2/3 of the measured TB37 trend can be accounted for by the 1992–2005 water vapor trend. The TMR algorithm results suggest that the added component contributing to the upward TB37 trend is a combination of CLW and precipitation. A significant contribution due to a global wind speed increase appears less likely but cannot be ruled out.

8. Summary/Discussion

[38] The continuous 1992–2005 data record of the TOPEX Microwave Radiometer has been reprocessed to produce both integrated water vapor and cloud liquid water archives from overocean microwave brightness temperature measurements. The reprocessing removes instrument-induced TB drifts, a step critical for estimating long-term climate trends. The instrument drifts were identified and removed using the vicarious cold reference method, a standard demonstrated to be robust in the presence of plausible climate variations. Results for long-term trends of IWV and CLW were presented for global, zonal, and regional stratifications.

[39] The most important result of the TMR-based trends analyses is the confirmation of the global scale IWV trends derived by previous investigators from the interleaved data sets of SSM/I instruments. Our own comparisons based on 1992–2005 data, clearly illustrate the agreement between TMR and SSM/I. On a global scale, the SSM/I- and TMR-derived IWV trends differ by less than 0.3%/decade, approximately one sixth of the measured trends. For the tropics, tracking of IWV variations on both seasonal and decadal time scales demonstrates relative precision at the 0.1–0.2 mm level. These results are not sensitive to the platform-dependent local time-of-day effects expected of the sun-synchronous SSM/I measurements. The long-term IWV trend agreement between these two very different satellite instruments attests to the calibration stability of both, and provides confidence that current microwave radiometer technology and processing tools are capable of measuring decadal scale tropospheric water vapor trends at the levels needed for meaningful climate monitoring. The TMR and SSM/I results consistently demonstrate that global ocean water vapor has been increasing at a rate between 1.0 and 1.8%/decade over nearly a 20 year interval through 2005. The range of uncertainty is largely reflective of the difficulties of extracting very small decade-scale trends from satellite data that are less than two decades in duration and sensitive to global scale transient effects such as ENSO events and volcanic eruptions. The extension of high-quality satellite monitoring of ocean water vapor trends over the next 10–20 years will very likely produce a tighter observational constraint for climate change modeling. The successors to TMR, the microwave radiometers associated with the Jason-1 and Jason-2 altimetry missions, should be well positioned to extend the water vapor trends through 2012 or beyond. Six months of overlapping observations in tandem orbits with ~60 s offset between TOPEX/Jason-1 and Jason-1/Jason-2 provides optimal calibration continuity for merging multiple instrument time series.

[40] In addition to the global and hemispheric scale results, the TMR archive was stratified to illustrate the latitude and regional dependence of IWV trends. The results reveal that the 1–2%/decade global- and hemisphere-averaged trends were the product of highly variable regional trends, ranging from ~−8 to +8%/decade. Latitude variations of the IWV trends showed clear peaks in both hemispheres near 40°S and 40°N, with a clear minimum near 10°S latitude. A comparison was also made between the latitude dependencies of IWV and SST trends over the 1992–2005 interval. The result was consistent with an 11%/K scaling of IWV/SST trends, in agreement with correlations seen at shorter time scales and consistent with a constant relative humidity model with amplified variations of air temperature relative to SST.

[41] TMR-based estimates of global scale CLW averages reveal fractional trends that are comparable to those of the IWV. However, the CLW trend estimates are not nearly as robust as for IWV. The statistical uncertainties are only marginally significant at the 2σ level and the effects of shorter 2 year trends at the beginning and end of the TMR archive are large. In addition, unmodeled precipitation effects as well as aliasing from wind speed trends may be contributing to the derived TMR CLW trend. In this regard, the most that can be stated is that the well constrained brightness temperature trend in the 37 GHz channel cannot be explained by the IWV trend alone. Small positive trends in cloud liquid plus precipitation and/or wind speed are indicated on a global scale. The individual brightness temperature trends of all three TMR channels are consistent with the retrieved trends in IWV and CLW plus precipitation with no measurable contribution from wind speed.

[42] The consistency of the TMR/SSM/I IWV results suggests that the climate data record from TMR and its successor radiometers on Jason-1 and Jason-2 should be considered as contributors to global data assimilation sys-

tems. Leading operational data assimilation centers such as NCEP and ECMWF have been including SSM/I retrievals in their assimilations since the 1990s [e.g., *Kalnay et al.*, 1996; *Kanamitsu et al.*, 2002]. In recent years, both NCEP and ECMWF, as well as other assimilation systems such as MERRA in NASA GMAO, have started to directly assimilate SSM/I radiances into their systems [*Bauer et al.*, 2006a, 2006b]. These additions have led to generally improved forecasting skills and forward modeling results. For example, *Okamoto and Derber* [2006] report reduced overall precipitation spin up as well as improved hurricane track assimilation because of the direct assimilation of SSM/I data. TMR observes similar radiance quantities as SSM/I, but with significantly different temporal sampling patterns (precessing orbit versus sun-synchronous). The previous experience with SSM/I makes it relatively straightforward to include TMR in the assimilation system. If accomplished, the two radiance data sets could complement and verify one another, providing improved constraints for reanalysis results over the 1992–2005 interval.

[43] **Acknowledgments.** The research described in this paper was carried out at the Jet Propulsion Laboratory, California Institute of Technology, under a contract with the National Aeronautics and Space Administration. Unnamed reviewer comments proved extremely valuable in the production of the published version of this paper.

References

Aumann, H. H., D. T. Gregorich, S. E. Broberg, and D. A. Elliott (2007), Seasonal correlations of SST, water vapor, and convective activity in tropical oceans: A new hyperspectral data set for climate model testing, *Geophys. Res. Lett.*, *34*, L15813, doi:10.1029/2006GL029191.

Bauer, P., P. Lopez, A. Benedetti, D. Salmond, and E. Moreau (2006a), Implementation of 1D + 4D-Var assimilation of precipitation-affected microwave radiances at ECMWF. Part I: 1D-Var, *Q. J. R. Meteorol. Soc.*, *132*(620), 2277–2306, doi:10.1256/qj.05.189.

Bauer, P., P. Lopez, D. Salmond, A. Benedetti, S. Saarinen, and M. Bonazzola (2006b), Implementation of 1D + 4D-Var assimilation of precipitation-affected microwave radiances at ECMWF. Part II: 4D-Var, *Q. J. R. Meteorol. Soc.*, *132*(620), 2307–2332.

Bony, S., et al. (2006), How well do we understand and evaluate climate feedback processes?, *J. Clim.*, *19*, 3445–3482, doi:10.1175/JCLI3819.1.

Brown, S., and C. Ruf (2005), Determination of an Amazon hot reference target for the on-orbit calibration of microwave radiometers, *J. Atmos. Oceanic Technol.*, *22*(9), 1340–1352, doi:10.1175/JTECH1769.1.

Brown, S., S. Desai, S. Keihm, and W. Lu (2009), Microwave radiometer calibration on decadal time scales using on-earth brightness temperature references: Application to the TOPEX Microwave Radiometer, *J. Atmos. Oceanic Tech.*, doi: 10.1175/2009JTECHA1305.1, in press.

Fletcher, N. H. (1962), *The Physics of Rainclouds*, pp. 386, New York, Cambridge Univ. Press, Cambridge, U. K.

Harries, J. E., and J. M. Futyan (2006), On the stability of the Earth's radiative energy balance: Response to the Mt. Pinatubo eruption, *Geophys. Res. Lett.*, *33*, L23814, doi:10.1029/2006GL027457.

Held, I. M., and B. J. Soden (2000), Water vapor feedback and global warming, *Annu. Rev. Energy Environ.*, *25*, 441–475, doi:10.1146/annurev.energy.25.1.441.

Held, I. M., and B. J. Soden (2006), Robust responses of the hydrological cycle to global warming, *J. Clim.*, *19*, 5686–5699, doi:10.1175/JCLI3990.1.

Hilburn, K. A., and F. J. Wentz (2008), Intercalibrated passive microwave rain products from the United Microwave Ocean Retrieval Algorithm (UMORA), *J. Appl. Meteorol. Climatol.*, *47*(3), 778–794, doi:10.1175/2007JAMC1635.1.

Houghton, J. T., L. G. Filho, B. A. Callander, N. Harris, A. Kattenberg, and K. Maskell (Eds.) (1996), *Climate Change 1995: The Science of Climate Change*, 572 pp., Cambridge Univ. Press, Cambridge, U. K.

Janssen, M. A., C. S. Ruf, and S. J. Keihm (1995), TOPEX/Poseidon Microwave Radiometer (TMR): Part II. Antenna pattern correction and brightness temperature algorithm, *IEEE Trans. Geosci. Remote Sens.*, *33*, 138–146, doi:10.1109/36.368214.

Kalnay, E., et al. (1996), The NCEP/NCAR 40-year reanalysis project, *Bull. Am. Meteorol. Soc.*, *77*(3), 437–471, doi:10.1175/1520-0477(1996)077<0437:TNYRP>2.0.CO;2.

Kanamitsu, M., W. Ebisuzaki, J. Woollen, S.-K. Yang, J. J. Hnilo, M. Fiorino, and G. L. Potter (2002), NCEP-DOE AMIP-II reanalysis (R-2), *Bull. Am. Meteorol. Soc.*, *83*(11), 1631–1643, doi:10.1175/BAMS-83-11-1631(2002)083<1631:NAR>2.3.CO;2.

Keihm, S. J., and C. S. Ruf (1995), The role of water vapor radiometers for in-flight calibration of the TOPEX Microwave Radiometer, *Mar. Geod.*, *18*, 139–156, doi:10.1080/15210609509379749.

Keihm, S. J., M. A. Janssen, and C. S. Ruf (1995), TOPEX/Poseidon Microwave Radiometer (TMR): Part III. Wet troposphere range correction algorithm and pre-launch error budget, *IEEE Trans. Geosci. Remote Sens.*, *33*, 147–161, doi:10.1109/36.368213.

Keihm, S. J., V. Zlotnicki, and C. S. Ruf (2000), TOPEX microwave radiometer performance evaluation, 1992–1998, *IEEE Trans. Geosci. Remote Sens.*, *38*, 1379–1386, doi:10.1109/36.843032.

Kistler, R., et al. (2001), The NCEP-NCAR 50-year reanalysis: Monthly means CD–ROM and documentation, *Bull. Am. Meteorol. Soc.*, *82*(2), 247–267, doi:10.1175/1520-0477(2001)082<0247:TNNYRM>2.3.CO;2.

Lin, B., and W. B. Rossow (1994), Observations of cloud liquid water path over oceans: Optical and microwave remote sensing methods, *J. Geophys. Res.*, *99*(D10), 20,907–20,927, doi:10.1029/94JD01831.

Malkevich, M. S., V. S. Kosopalov, and V. I. Skatskiy (1981), Statistical characteristics of the vertical water content structure of cumulus clouds, *Izv. Russ. Acad. Sci. Atmos. Oceanic Phys, Engl. Transl.*, *17*(3), 203–210.

Mitchum, G. T. (1998), Monitoring the stability of satellite altimeters with tide gauges, *J. Atmos. Oceanic Technol.*, *15*(3), 721–730, doi:10.1175/1520-0426(1998)015<0721:MTSOSA>2.0.CO;2.

Njoku, E. G., J. M. Stacey, and F. T. Barath (1980), The Seasat scanning multichannel microwave radiometer (SMMR): Instrument description and performance, *IEEE J. Oceanic Eng.*, *5*, 100–115, doi:10.1109/JOE.1980.1145458.

Obligis, E., L. Eymard, and N. Tran (2007), A new sidelobe correction algorithm for microwave radiometers: Application to the Envisat instrument, *IEEE Trans. Geosci. Remote Sens.*, *45*, 602–612, doi:10.1109/TGRS.2006.887165.

O'Dell, C. W., F. J. Wentz, and R. Bennartz (2008), Cloud liquid water path from satellite-based passive microwave observations: A new climatology over the global oceans, *J. Clim.*, *21*(8), 1721–1739, doi:10.1175/2007JCLI1958.1.

Okamoto, K., and J. C. Derber (2006), Assimilation of SSM/I radiances in the NCEP Global Data Assimilation System, *Mon. Weather Rev.*, *134*(9), 2612–2631, doi:10.1175/MWR3205.1.

Ruf, C. S. (2000), Detection of calibration drifts in spaceborne microwave radiometers using a vicarious cold reference, *IEEE Trans. Geosci. Remote Sens.*, *38*, 44–52, doi:10.1109/36.823900.

Ruf, C. S., S. J. Keihm, B. Subramanya, and M. A. Janssen (1994), TOPEX/Poseidon Microwave Radiometer performance and in-flight calibration, *J. Geophys. Res.*, *99*, 24,915–24,926, doi:10.1029/94JC00717.

Ruf, C. S., S. J. Keihm, and M. A. Janssen (1995), TOPEX/Poseidon Microwave Radiometer (TMR): Part I. Instrument description and antenna temperature calibration, *IEEE Trans. Geosci. Remote Sens.*, *33*, 125–137, doi:10.1109/36.368215.

Santer, B. D., T. M. L. Wigley, J. S. Boyle, D. J. Gaffen, J. J. Hnilo, D. Nychka, D. E. Parker, and K. E. Taylor (2000), Statistical significance of trends and trend differences in layer-average atmospheric temperature time series, *J. Geophys. Res.*, *105*(D6), 7337–7356, doi:10.1029/1999JD901105.

Santer, B. D., et al. (2007), Identification of human-induced changes in atmospheric moisture content, *Proc. Natl. Acad. Sci. U. S. A.*, *104*(39), 15,248–15,253, doi:10.1073/pnas.0702872104.

Schneider, E. K., B. P. Kirtman, and R. S. Lindzen (1999), Tropospheric water vapor and climate sensitivity, *J. Atmos. Sci.*, *56*, 1649–1658, doi:10.1175/1520-0469(1999)056<1649:TWVACS>2.0.CO;2.

Soden, B. J., and I. M. Held (2006), An assessment of climate feedbacks in coupled ocean-atmosphere models, *J. Clim.*, *19*, 3354–3360, doi:10.1175/JCLI3799.1.

Soden, B. J., and S. R. Schroeder (2000), Decadel variations in tropical water vapor: A comparison of observations and a model simulation, *J. Clim.*, *13*, 3337–3341, doi:10.1175/1520-0442(2000)013<3337:DVITWV>2.0.CO;2.

Soden, B. J., R. T. Wetherald, G. L. Stenchikov, and A. Robock (2002), Global cooling after the eruption of Mount Pinatubo: A test of climate feedback by water vapor, *Science*, *296*, 727–730, doi:10.1126/science.296.5568.727.

Soden, B. J., D. L. Jackson, V. Ramaswamy, D. Schwarzkopf, and X. Huang (2005), The radiative signature of upper tropospheric moistening, *Science*, *310*, 841–844, doi:10.1126/science.1115602.

Stephens, G. L., and C. D. Kummerow (2007), The remote sensing of clouds and precipitation from space: A review, *J. Atmos. Sci.*, *64*(11), 3742–3765, doi:10.1175/2006JAS2375.1.

Swanson, P. N., and A. L. Riley (1980), The Seasat scanning multichannel microwave radiometer (SMMR): Radiometric calibration algorithm development and performance, *IEEE J. Oceanic Eng.*, *5*, 116–124, doi:10.1109/JOE.1980.1145452.

Taylor, P. K., K. B. Katsaros, and R. G. Lipes (1981), Determinations by Seasat of atmospheric water and synoptic fronts, *Nature*, *294*, 737–739, doi:10.1038/294737a0.

Tran, N., D. Vandemark, C. Ruf, and B. Chapron (2002), The dependence of nadir ocean surface emissivity on wind vector as measured with TMR, *IEEE Trans. Geosci. Remote Sens.*, *40*(2), 515–523, doi:10.1109/36.992827.

Trenberth, K. E., J. Fasullo, and L. Smith (2005), Trends and variability in column-integrated atmospheric water vapor, *Clim. Dyn.*, *24*, 741–758, doi:10.1007/s00382-005-0017-4.

Trenberth, K. E., B. Moore, T. R. Karl, and C. Nobre (2006), Monitoring and prediction of the Earth's climate: A future perspective, *J. Clim.*, *19*, 5001–5008.

Wentz, F. J., and M. Schabel (2000), Precise climate monitoring using complementary satellite data sets, *Nature*, *403*, 414–416, doi:10.1038/35000184.

Wentz, F. J., L. Ricciardulli, K. Hilburn, and C. Mears (2007), How much more rain will global warming bring?, *Science*, *317*, 233–235, doi:10.1126/science.1140746.

Wilheit, T. T. (1979), A model for the microwave emissivity of the ocean's surface as a function of wind speed, *IEEE Trans. Geosci. Electron.*, *17*, 244–249, doi:10.1109/TGE.1979.294653.

S. Brown, S. Desai, E. Fetzer, S. Keihm, W. Lu, and J. Teixeira, Jet Propulsion Laboratory, California Institute of Technology, 4800 Oak Grove Drive, Pasadena, CA 91109, USA. (stephen.j.keihm@jpl.nasa.gov)

X. Huang and C. Ruf, Department of Atmospheric, Oceanic and Space Sciences, University of Michigan, 2455 Hayward Street, Ann Arbor, MI 48109-2143, USA.

Y. Yung, Division of Geological and Planetary Sciences, California Institute of Technology, Mail Stop 150-21, Pasadena, CA 91125, USA.